Heliyon 10 (2024) e37245

Contents lists available at ScienceDirect

Heliyon

journal homepage: www.cell.com/heliyon

Research article

Spatio-temporal dynamics and influencing factors of carbon emissions (1997–2019) at county level in mainland China based on DMSP-OLS and NPP-VIIRS Nighttime Light Datasets

Nina Zhu [a], Xue Li [b], Sibo Yang [c,*], Yi Ding [a], Gang Zeng [d]

[a] School of Event and Communication, Shanghai University of International Business and Economics, Shanghai, 201620, China
[b] School of International Economics and Trade, Shanghai Lixin University of Accounting and Finance, 201620, China
[c] Department of Public and International Affairs, City University of Hong Kong, 999077, Hong Kong, China
[d] The Center for Modern Chinese City Studies & Institute of Urban Development, East China Normal University, Shanghai, 200062, China

ARTICLE INFO

Keywords:
Nighttime light data
Deep learning method
Carbon emissions
Heterogeneity
County-level
Influencing factors

ABSTRACT

Global warming caused by extensive carbon emissions is a critical global issue. However, the lack of county-level carbon emissions data in China hampers comprehensive research. To bridge this gap, we employ a deep learning method on nighttime light data sets to estimate county-level carbon emissions in mainland China from 1997 to 2019. Our key contributions include the successful derivation of more reliable data, revealing the evolution of spatial dynamics and emissions epicenters. Moreover, we identify a novel inverted N-shaped relationship between gross domestic product per capita and carbon emissions in the eastern and western regions, as well as an N-shaped relationship in the central region, challenging mainstream wisdom. Additionally, we highlight the significant impacts of population density, industrial structure, and carbon intensity on carbon emissions. Our study also unveils the nuanced effects of government spending, which exhibits both inhibitory and region-specific influences. These findings serve to enhance our understanding of the factors influencing carbon emissions and contribute to informed decision-making in addressing climate change-related challenges.

1. Introduction

Global warming caused by massive carbon emissions (CE) has resulted in more frequent extreme climate events, posing great challenges to the ecological environment as well as human development and survival [1]. As the largest developing country in the world, while pursuing rapid economic development, China presents a large number of economic activities with "high input, high consumption, and low output", resulting in China's total energy production and consumption ranking first in the world. The resulting CE accounted for 30.9 % of the global total in 2020 [2]. To this end, China clearly stated, at the 75th UN General Assembly in September 2020, that it aims to achieve the goals of "carbon peaking" by 2030 and "carbon neutrality" by 2060 [3]. There are many researches foucus on CE, including CE accounts, drivers of CE, CE forecasting, and more [4–7]. However, most of them have concentrated on the national level, provincial level, and city level. Actually, CE may be spatially heterogeneous, even within the same city; this is especially notable in China, due to its large area [8]. In China, the county is a basic spatial unit with complete economic

* Corresponding author.
E-mail address: 3314681@163.com (S. Yang).

https://doi.org/10.1016/j.heliyon.2024.e37245
Received 17 May 2024; Received in revised form 12 August 2024; Accepted 29 August 2024
Available online 30 August 2024

functions and relatively independent operation in China. It is also an important part of China's CE and the main bearing space for carbon sink functions, making it a key administrative unit for the implementation of the dual carbon goals and policies. Therefore, studying CE at the county level is of great significance for the reduction of CE and the formulation of related policies.

Previous studies on CE account at the county level have mainly been based on statistical data and conducted accounting through the CE coefficient method [9]. For example, Long et al. [10] have systematically estimated the CE of Changxing County from four aspects according to the Intergovernmental Panel on Climate Change (IPCC) National Greenhouse Gas Inventory Guidelines. Based on land-use data and CE coefficients, Cao and Yuan [11] have estimated the direct and indirect CE associated with land-uses in 38 counties in Chongqing in China during the period of 1997–2015. Guan et al. [12] have calculated CO2 emissions from energy consumption for 18 counties in Ningxia used carbon emission coefficient method. The estimation of county CE in all of these studies were based on publicly available statistics; however, accounting for CE is difficult for counties that do not have statistics related to carbon emissions.

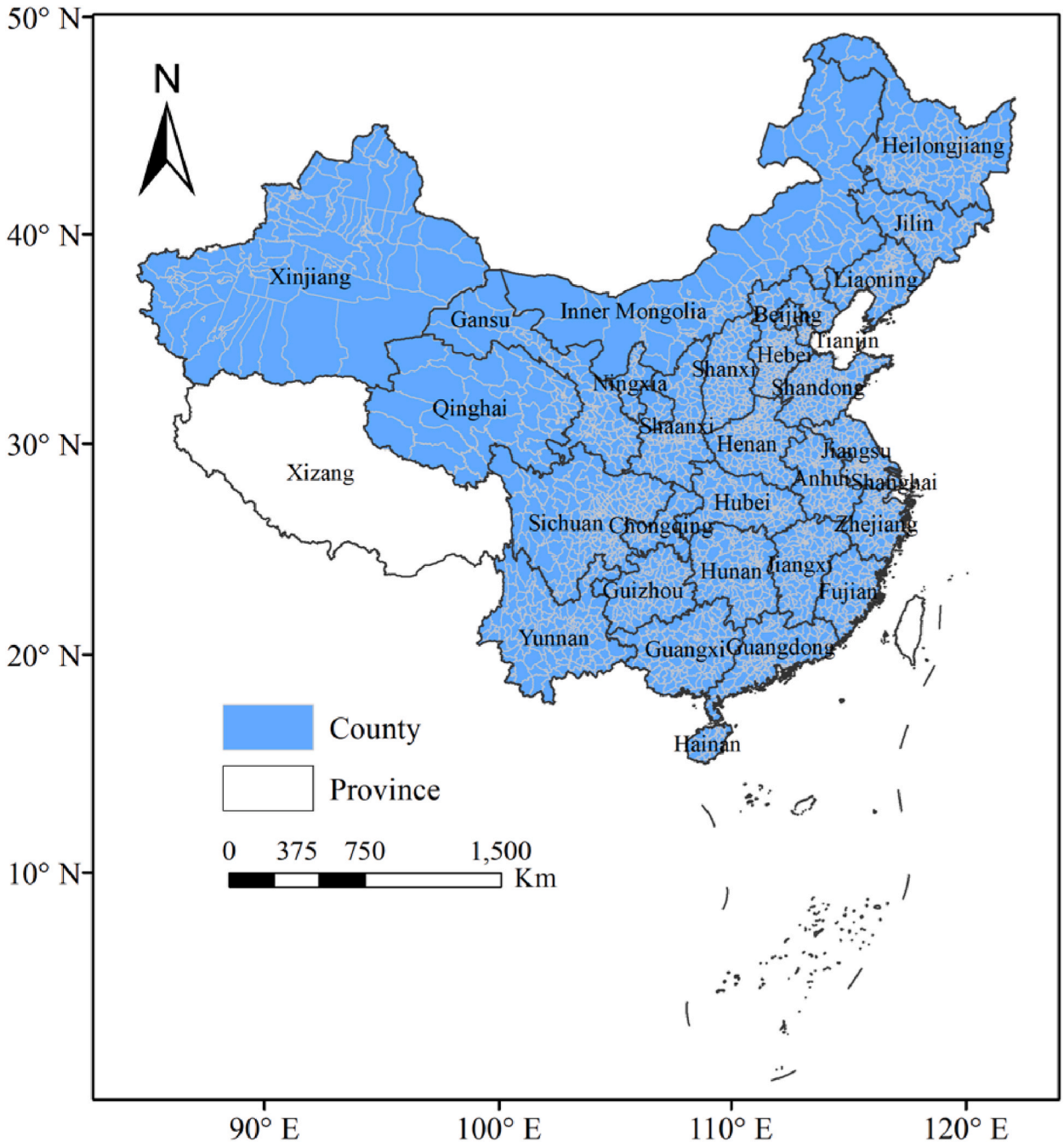

Fig. 1. The location of the study area.

With the development of remote sensing technology, nighttime light remote sensing data has begun to be used for the estimation of CE on a smaller spatial scale [13]. At present, the most-used nighttime light data are the DMSP-OLS data obtained by the operational linesman system (OLS) carried by the U.S. defense meteorological satellite program (DMSP) and the data obtained by the visible infrared imaging radiometer suite (VIIRS) carried by the Suomi national polar-orbiting partnership (Suomi-NPP). However, relevant CE application research mainly used a single data set for there are significant differences between the DMSP-OLS and NPP-VIIRS datasets in terms of time range, spatial resolution, and sensor characteristics. For example, the time range of the DMSP-OLS dataset is from 1992 to 2013, while the NPP-VIIRS dataset has been available since 2012. In addition, the spatial resolution of the DMSP-OLS dataset is 1 km, while the NPP-VIIRS has a higher resolution of 500 m. The sensors of the two also have different photosensitive characteristics, resulting in discrepancies in nighttime light intensity values between the two datasets for the same regions and time periods. These differences have an important impact on CE estimates because they may lead to inconsistencies between different data sources, thereby affecting the accuracy of the estimated results. Therefore, when using these data for CE estimates, consistency corrections must be performed to ensure the reliability of the results. As such, there are relatively few concordance-corrected researches for the two datasets [14,15]. Or, just integrated them based on a simple statistical relationship [16–18], and the intrinsic non-linear transformation relationship between them has not been effectively identified, resulting in low accuracy of consistency correction. Therefore, it is very important to continuously improve the integrated accuracy of these two types of nighttime light data for the construction of long-term and high-precision CE data. Machine learning methods provide new ideas for integration of them. Compared with traditional methods, deep learning methods have strong learning abilities, better simulation and prediction results, and can effectively identify the non-linear relationships between different elements. Therefore, this study paper attempts to use deep learning methods for consistency correction of DMSP-OLS and NPP-VIIRS. On this basis, high-precision and long time-series of CE for counties in China are obtained, provideing a basis for the study of CE at a finer scale.

On the other hand, numerous studies have analyzed the influencing factors of CE on the national, provincial, and the prefecture-level city scales. Due to data limitations, research on the influencing factors of CE at the county level remains relatively limited, and the research scope has mostly been concentrated in certain small areas, such as the Yellow River Delta, Yangtze River Delta, Beijing-Tianjin-Hebei, Zhejiang province, and so on [19]. However, further research is needed on the influencing factors of CE and their spatiotemporal heterogeneity at the county scale over the entire Chinese mainland is still needed.

Thus, our research gets the following marginal contributions: (1) we used a deep learning method to unify the scale of DMSP-OLS and NPP-VIIRS images and calculated 2875 county-level energy-related CE for the period 1997–2019, the fitting effects of which are better than those obtained in previous studies based on traditional statistical method and traditional machine learning methods; (2) we find that, at the county scale, government spending has a significant inhibitory effect on CE in the eastern and central regions, while the effect on CE in the western region is insignificant. Gross domestic product per capita presents an inverted N-shaped relationship with CE in the eastern and western regions, and an N-shaped relationship in the central region. These findings enrich the literature on factors influencing CE at smaller scales.

2. Study area and data source

2.1. Study area

In this study, mainland China is the research object (excluding Hong Kong, Macao, and Xizang), encompassing 30 provinces and 2875 counties (Fig. 1). China spans from 73°33′E to 135°05′E longitude and from 3°51′N to 53°33′N latitude, covering about 9.6 million square kilometers.

2.2. Data source

DMSP-OLS and NPP-VIIRS nighttime light data were sourced from the U.S. National Geophysical Data Center (NGDC, https://ngdc.noaa.gov/). There are two types of DMSP-OLS nighttime light data: version 4 DMSP-OLS nighttime light images and global radiance calibrated nighttime light images. The existing version 4 DMSP-OLS images data sets include 34 images from 1992 to 2013 acquired by 6 different DMSP satellites. Each period of the DMSP-OLS nighttime light images includes three types of annual average images: Cloud-free coverages, average visible, and stable lights images. Stable light images include city, town, and other persistent light sources, with the effects of occasional noise such as moonlight, sparks, and oil and gas burning having been removed. The reference frame of the image is the WGS-84 coordinate system with a spatial resolution of 30 arcseconds. The digital number (DN) of the image represents the average light intensity, with values ranging from 0 to 63. An area with a DN of 0 is a no-light area and the larger the DN, the greater the light intensity of the area. Compared with the stable light images, the radiance-calibrated nighttime light images solve the problem of saturation of the pixel values; therefore, they can be used as an ideal reference image in relevant research. Therefore, we selected 34 periods of stable light images from 1992 to 2013 obtained by 6 different DMSP satellites and all 8 periods of global radiation-calibrated nighttime light images.

The NPP-VIIRS nighttime light image was captured by the Suomi-NPP satellite using the Visible Infrared Imaging Radiometer (VIIRS) with a spatial resolution of 15 arcseconds, which is better than that of the DMSP-OLS sensor. In addition, the images do not suffer from the saturation of pixel values, but there are still negative and unusually abrupt pixel values, as they have not been processed to mask out auroras, fires, boats, and other noise [17]. Due to the difference in performance between the DMSP and NPP-VIIRS sensors, the pixel values of the two nighttime light data sets are quite different. The time scale of NPP-VIIRS is from 2012 to the present, including monthly and annual data. Among them, the NOAA/NGDC released two periods of the standard annual nighttime light image

in 2015 and 2016, with unstable light sources and background noise removed. Therefore, the images from these two years can be used as a reference to correct images from other years [20]. Therefore, in this study, we selected monthly images from 2012 to 2019 and annual images from 2015 to 2016.

Although the DMSP-OLS dataset has the problem of pixel saturation, it provides a long time series from 1992 to 2013, which is essential for analyzing the spatiotemporal dynamics of carbon emissions. By covering multiple years of data, we are able to capture long-term trends and changes instead of relying on short-term data, which improves the robustness of the results. The NPP-VIIRS dataset has a high spatial resolution, which can more accurately capture light source changes and reduce the saturation problem in the DMSP-OLS dataset. In this study, we used deep learning methods to perform consistency correction on DMSP-OLS and NPP-VIIRS. With this method, we combined the advantages of both datasets, effectively improving the accuracy and reliability of carbon emission estimates. Deep learning methods are able to handle complex nonlinear relationships and reduce potential errors by improving data consistency correction. This data integration and method application significantly improved the robustness of the research results and provided a solid foundation for high-precision carbon emission data.

The vector data of China's county-level administrative regions used in this study were obtained from the national 1:4,000,000 databases of the National Geomatics Center of China (http://www.ngcc.cn) in 2018, and the energy consumption data were obtained from the *China Energy Statistical Yearbook*, issued by the National Bureau of Statistics of China (see Table 1).

3. Method

3.1. Multilayer perceptron

In this study, the neural network method was mainly used to unify DMSP-OLS and NPP-VIIRS nighttime light datasets to invert long-time CE data at the county level. The transformation relationship between different types of nighttime light image data is nonlinear [18]. Compared to traditional statistical methods and shallow neural network, the deep learning method has the ability to learn hidden relationships in the elements and can effectively simulate the complex nonlinear relationship between elements. Also, it does not impose any restrictions on the input variables.

Multilayer perceptron (MLP) is a type of deep learning method. It is a single-layer perceptron based on the addition of hidden layers, increase the number of hidden layers so that it has more neuron layers, so it is also known as deep neural networks, deeper network structure makes the original unprocessed and individually uninterpretable feature extraction is particularly effective, has been widely used in large amounts of data feature extraction prediction [21]. MLP consists of an input layer, an output layer and a hidden layer. Each hidden layer consists of a defined number of neurons, and the neurons of the MLP are connected in a way that there are no intra-layer connections and all inter-layer connections. In a multilayer perceptron, each neuron is connected to all the neurons in the previous layer and each connection has a weight [22]. Each neuron takes the signals passed from the previous layer and performs a weighted sum and then goes through an activation function to produce an output [22]. The activation functions for the hidden and output layers are usually nonlinear, such as Sigmoid, ReLU, Tanh, etc., in order to allow the network to capture nonlinear relationships. Fig. 2 is a schematic diagram of the structure of an MLP with three hidden layers.

3.2. Moran's I

Moran's *I* was used to investigate the spatial correlation of CE at the county level in mainland China in this study. It measures the similarity of the attribute values of CE in adjacent regions of space [23]. The global Moran's *I* is as follows:

$$I = \frac{n\sum_{i=1}^{n}\sum_{j\neq i}^{n} W_{ij}(x_i-\overline{x})(x_j-\overline{x})}{\sum_{i=1}^{n}\sum_{j\neq i}^{n} W_{ij}(x_i-\overline{x})^2} = \frac{n\sum_{i=1}^{n}\sum_{j\neq i}^{n} W_{ij}(x_i-\overline{x})(x_j-\overline{x})}{S^2\sum_{i=1}^{n}\sum_{j\neq i}^{n} W_{ij}}$$

where I is the Moran index: $S^2 = \frac{1}{n}\sum_{i}(x_i-\overline{x})^2$, $\overline{x} = \frac{1}{n}\sum_{i=1}^{n} x_i$. The value of Moran's *I* fluctuates between −1 and 1. If Moran's *I* is greater

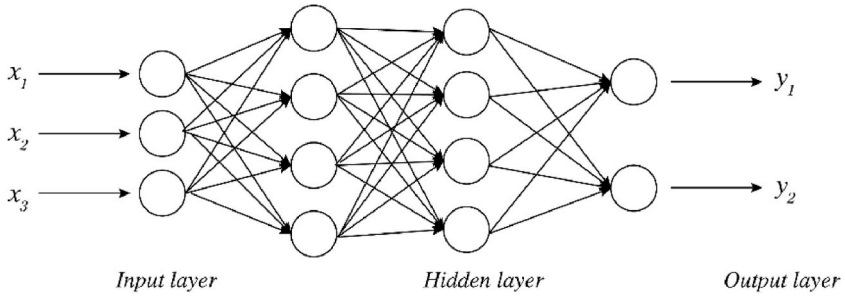

Fig. 2. The topology of the MLP.

than 0, showing that CE is positive in space. If Moran's *I* is less than 0, showing that CE is negative in space. There is no spatial correlation if Moran's *I* is equal to 0.

3.3. Spatial STIRPAT model

The Stochastic Impacts by Regression on Population, Affluence, and Technology (STIRPAT) model is used to investigate the influencing factors of CE at the county level. The STIRPAT model has been widely used to explore CE [24,25].

The basic equation of the STIRPAT model is:

$$I_i = \alpha P_i^b A_i^c T_i^d e_i$$

where *I* represents the environmental pressure, *P* represents the demographic factors, *A* is the wealth, and *T* is the technology; α is a coefficient; *b*, *c*, and *d* are the indices of demographic factors, wealth, and technology, respectively; *e* is a random influencing factor; and *i* is the different observation units. According to previous studies, People density (PD), Carbon intensity (CI), Industrial structure (IS), Government spending (GS), and Gross domestic product per capita (PGDP) were selected as the influencing factors of CE, and all of them are from the *China City Statistical Yearbook*. To further analyzing the impact of economic development on CE, we also introduce the quadratic and tertiary terms of PGDP. Furthermore, to weaken heteroscedasticity between variables, both sides of the STIRPAT model are taken logarithmically. Therefore, the modified STIRPAT model is as follows:

$$Ln\ EC_{it} = \alpha_0 + \alpha_1\ Ln\ PD_{it} + \alpha_2\ Ln\ CI_{it} + \alpha_3\ Ln\ IS_{it} + \alpha_4\ Ln\ GS_{it} + \alpha_5\ Ln\ PGDP_{it} + \alpha_6\ Ln\ PGDP_{it}^2 + \alpha_7\ Ln\ PGDP_{it}^3 + \varepsilon_{it}$$

The above model is a traditional measurement model. Considering the characteristics of CE with spatial correlation, and the traditional econometric model ignores the spatial correlation, this study uses a spatial econometric model. The general expression of the spatial econometrics model (Spatial Durbin Model, SDM) is:

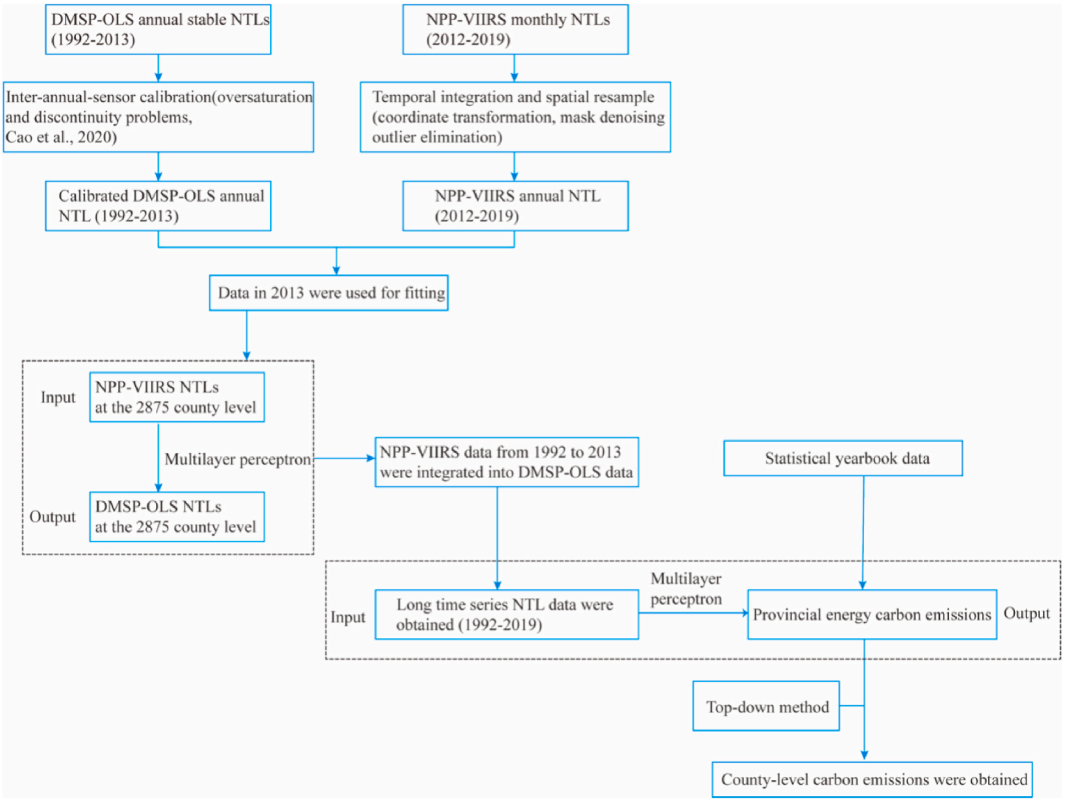

Fig. 3. The process of data fitting.
Note: NTL represents nighttime light.

$$Ln\,EC_{it} = \rho\sum_{j=1}^{n} W_{ijt}\,Ln\,EC_{it} + \alpha_1\,Ln\,PD_{it} + \alpha_2\,Ln\,CI_{it} + \alpha_3\,Ln\,IS_{it}$$
$$+\alpha_4\,Ln\,GS_{it} + \alpha_5\,Ln\,PGDP_{it} + \alpha_6\,Ln\,PGDP_{it}^2 + \alpha_7\,Ln\,PGDP_{it}^3 + \beta_1\sum_{i\neq j}^{n} W_{ijt}\,Ln\,PD_{it}$$
$$+\beta_2\sum_{i\neq j}^{n} W_{ijt}\,Ln\,CI_{it} + \beta_3\sum_{k=1}^{6} IS_{kit} + \beta_4\sum_{i\neq j}^{n} W_{ijt}\,Ln\,GS_{it} + \beta_5\sum_{i\neq j}^{n} W_{ijt}\,Ln\,PGDP_{it}$$
$$+\beta_6\sum_{i\neq j}^{n} W_{ijt}\,Ln\,PGDP_{it}^2 + \beta_7\sum_{i\neq j}^{n} W_{ijt}\,Ln\,PGDP_{it}^3 + \mu_i + \theta_i + \varepsilon_{it}$$

where i represents the region, t represents the time; W_{ijt} is the spatial weight matrix; ρ represents the spatial spillover coefficient of carbon emissions; α_1, α_2, …, α_7 and β_1, β_2, …, β_7 are parameters to be estimated; μ_i is the individual fixed effect, θ_i is the time-fixed effect; and ε_{it} is the random disturbance term.

4. Result

4.1. Inversion of county-level carbon emissions data sets based on DMSP-OLS and NPP-VIIRS

The process of carbon emissions data fitting is shown in Fig. 3.

There are problems of pixel over-saturation and discontinuity must in non-radiometrically calibrated DMSP-OLS nighttime light data. The pixel over-saturation means that the pixel digital number (DN value) exceeds the range of 0–63. If the actual DN value is greater than 63, it will be uniformly set to the highest threshold of 63. This can lead to indistinguishable gradients and details of the actual light intensity in some large urban centers to be lost. Therefore, according to the study of Cao et al. [26], we also adopts the classification correction method for stable light images across China based on the invariant target area to address the pixel over-saturation and discontinuity problems of non-radiometric calibrated DMSP-OLS nighttime light data. This method is more efficient for calibrating non-radiometric calibrated DMSP-OLS nighttime light data than previous methods [27,28].

There are negative or abnormal pixel values in NPP-VIIRS nighttime light data. Therefore, it also should be calibrated.

(1) Coordinate transformation:

As the original NPP-VIIRS nighttime light data are monthly data, in order to be consistent with the DMSP-OLS nighttime light data, it is necessary to synthesize the monthly NPP-VIIRS data into annual data. As the data distortion in the NPP-VIIRS nighttime light data typically occur in the middle and high latitudes [29], and mostly appear in summer, we selected the annual nighttime light data synthesized from the nine periods of nighttime light data from January to May and September to December in the study area as the basic research data [20,30]. As the NPP-VIIRS nighttime light image data will be deformed variably at different latitudes, they were first projected to the Albers equal-area projection coordinate system, which is suitable for China. Then, using the resampling tool in ArcGIS 10.5, the spatial resolution of the NPP-VIIRS nighttime light images was resampled to 1000 m × 1000 m, consistent with the resolution of the DMSP-OLS nighttime light image data. Based on the vector data of the county-level administrative districts in China, the NPP-VIIRS nighttime light image data of the study area were obtained. Next, the NPP-VIIRS nighttime light data in the study area had to be de-noised and outlier pixel-corrected.

(2) Mask de-noising

The U.S. National Geophysical Data Center provides two standard annual NPP-VIIRS nighttime light images for 2015 and 2016. First, we binarized the standard annual nighttime light data in 2015 and 2016, which were multiplied with the synthesized annual light images in 2015 and 2016 to remove unstable light sources and background noise, in order to obtain stable nighttime light images in 2015 and 2016. Then, the synthesized annual nighttime light data from 2012 to 2015 were processed according to Equation (1) and the synthesized annual nighttime light data from 2016 to 2019 were processed according to Equation (2), in order to obtain a stable long-term sequence of images from 2012 to 2019.

$$DN = \begin{cases} 0, DN_i \leq 0 | DN_{i+1} = 0 \\ DN_i, Other \end{cases} \quad (1)$$

$$\mathrm{DN} = \begin{cases} 0,\ \mathrm{DN_i} \leq 0 | \mathrm{DN_{i\text{-}1}} = 0 \\ \mathrm{DN_i}, \mathrm{Other} \end{cases} \quad (2)$$

where DN represents the pixel value of the nighttime light image after correction, DN_i is the pixel value of the nighttime light image to be corrected, DN_{i+1} is the pixel value of the nighttime light image one year after correction, and DN_{i-1} is the nighttime light pixel value in the year before correction.

(3) Outlier elimination

In places with high surface emissivity, there are an abnormal pixel values which are much higher than the maximum values of pixels in the surrounding area and, so, do not conform to the actual situation. In order to ensure the accuracy of the nighttime light data, these abnormal values need to be eliminated. As the maximum DN value within the Chinese region does not exceed the maximum value for Beijing, Shanghai, Shenzhen, and Guangzhou [31], if a DN value is greater than this maximum DN value, it is replaced by the maximum DN value of its eight neighboring pixels. This process is repeated until all outliers larger than the maximum DN value of Beijing, Shanghai, Shenzhen, and Guangzhou are eliminated.

(4) Inter-calibration of DMSP-OLS and NPP-VIIRS nighttime light data

To obtain long-time nighttime light data, the DMSP-OLS and NPP-VIIRS data should be fused. First, we calculated the mean pixel values for the 2875 county-level units in mainland China based on DMSP-OLS and NPP-VIIRS in 2013 using the zonal statistical method in the ArcGIS 10.5 software, respectively. Then, the multilayer perceptron method was used to inter-calibrate the two datasets. And the country-level data of NPP-VIIRS was taken as an input layer and the country-level data of DMSP/OLS was taken as the output layer. According to the ratio of 8:2, we got a training data set and a test data set randomly. After continuous training, we got the optimal results (hidden layers = 3, neurons in each hidden layer = 10, iterations = 500, the activation function = Sigmoid).

The results are shown in Fig. 4. It can be seen that the correlation coefficients for the training set, test set, and overall set were 0.972, 0.958, and 0.970, respectively, which indicates that the multilayer perceptron method is advantageous for identifying the potential relationship between DMSP-OLS and NPP-VIIRS nighttime light data.

Next, we obtain the final simulated NPP-VIIRS data during 2014–2021 based on the annual increase rates of NPP-VIIRS data during 2013–2021. In summary, we obtained stable and continuous nighttime light data for the period 1997–2021, laying a foundation for further calculations of county-level CE.

Then, we explored the relationship between actual CE and nighttime light data at the province level using the multilayer perceptron. The simulation results are shown in Fig. 5, the correlation coefficients of the training set, test set, and overall set were 0.998, 0.994, and 0.998, respectively. Using the fused long-term nighttime light data (1997–2019), we calculated the total DN values in each province (30) and county (2875) and the weight of each county in its respective province. Next, we can simulate the CE in each

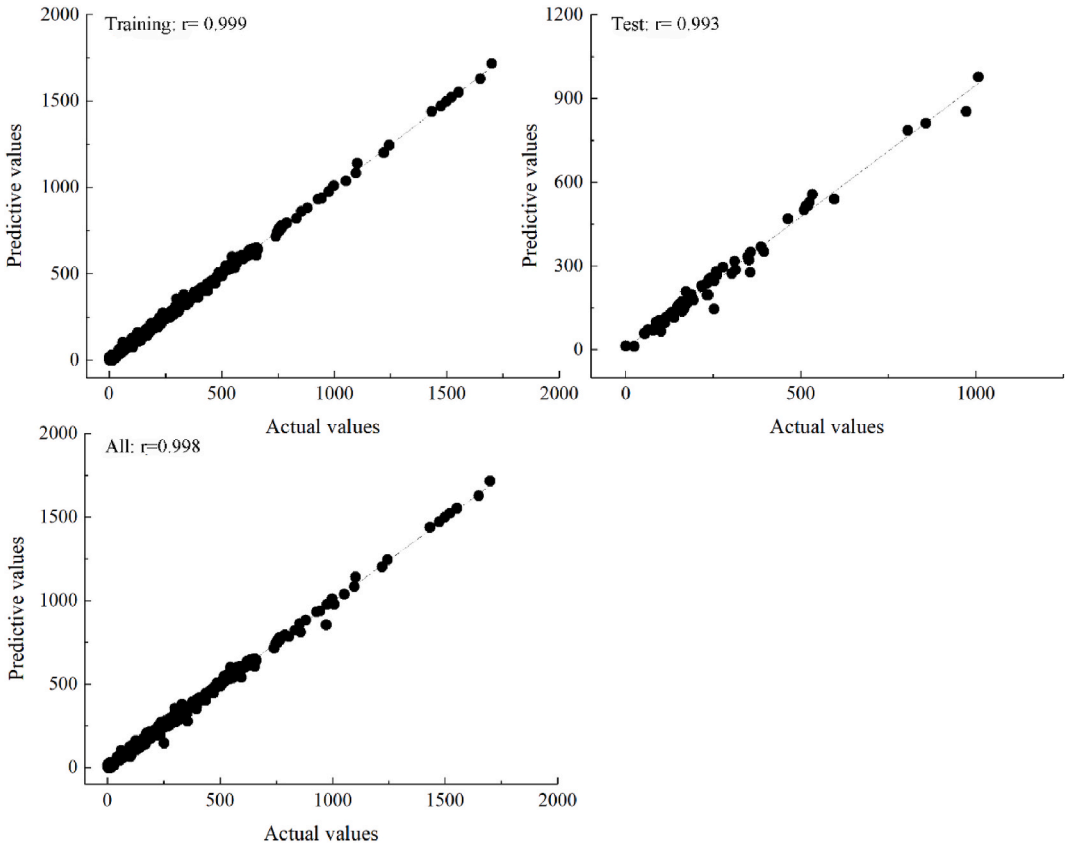

Fig. 4. The simulation results of the mean pixel values in 2013 between DMSP/OLS and NPP/VIIRS based on the MLP.

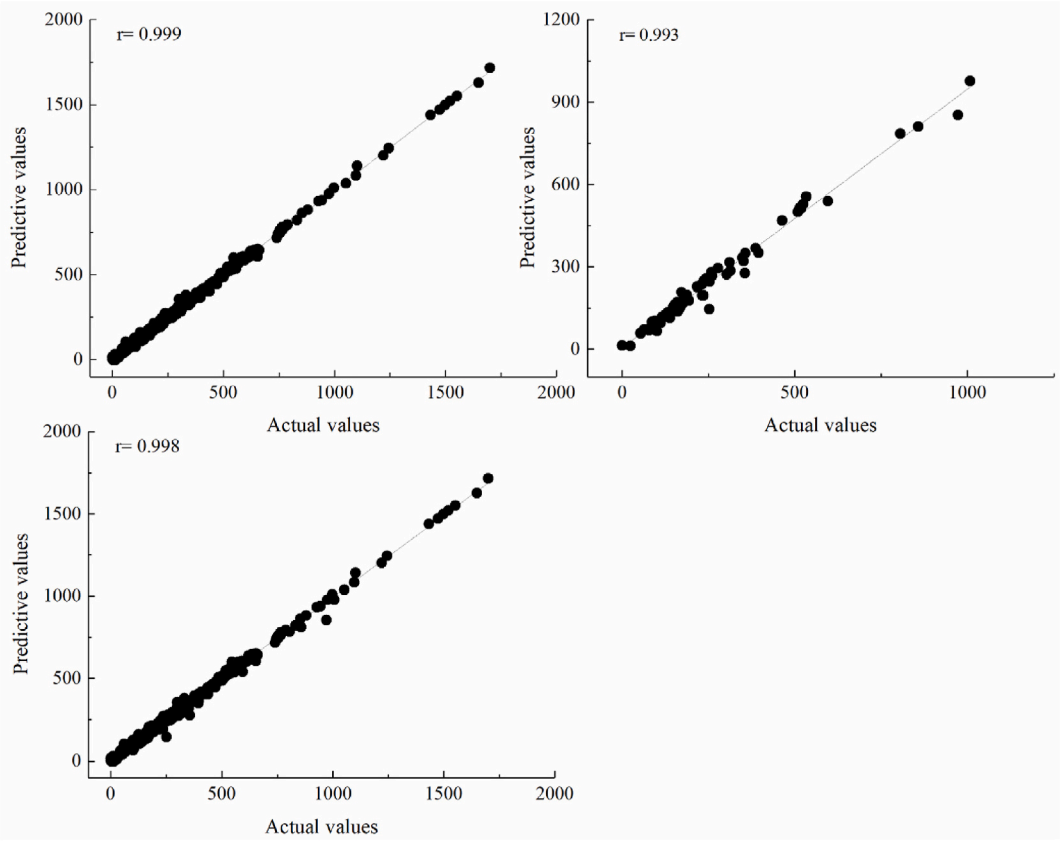

Fig. 5. The simulation results between actual provincial CE and the sum of pixel values at the province level for the training dataset, test dataset, and all datasets.

province using the trained MLP network. Finally, based on the concept of the top-down method, the weight of nighttime light in each county was multiplied by the CE of the province in which it is located, yielding the CE for each county [32–34]. At present, most existing studies focus on the analysis of CE at the national or provincial scale, and CE at the county scale is relatively scarce. This study provides important basic data for small-scale CE research. This work fills the gap in CE at the county scale and lays the foundation for future research at a finer granularity. Also, the application of deep learning methods provides new technical means for carbon emission measurement and demonstrates its potential in processing large-scale spatial data.

4.2. Spatiotemporal dynamics of carbon emissions

Based on the above results, we investigated the spatiotemporal changes of CE at the county level in mainland China. Table 2 shows the global Moran's *I* of CE from 2000 to 2019. All Moran's *I* were greater than 0, and their corresponding *p*-values all passed the 1 % significance test. The results shows that CE at the county level have a positive and significant spatial correlation. In addition, Moran's *I* showed a decreasing trend over time, which means that the spatial correlation of CE had begun to weaken (see Table 2).

Table 1
Description of each data source used in this study.

Data	Data Description	Year	Source
DMSP-OLS	Version 4 DMSP-OLS annual stable nighttime light data	1992–2013	https://ngdc.noaa.gov/eog/dmsp/downloadV4composites.html, accessed on October 20, 2022
NPP-VIIRS	Vision 1 NPP-VIIRS monthly vcm nighttime light data Annual VNL V1 nighttime light data	2012–2019 2015, 2016	https://eogdata.mines.edu/products/vnl/, accessed on October 20, 2022
Statistical data	Socioeconomic statistical data of county-level regions in mainland China	2000–2019	*China City Statistical Yearbook,* accessed on 15 November 2022
Energy data	Energy Statistical Data of province-level regions in mainland China	1997–2019	*China Energy Statistical Yearbook,* accessed on 15 November 2022
Boundaries	Shapefiles of county-level regions in mainland China	2018	National Geomatics Center of China (http://www.ngcc.cn), accessed on 15 November 2022

Table 2
The global Moran's *I* of CE at the county level in mainland China from 2000 to 2019.

Year	Moran's *I*	*p*-value	Year	Moran's *I*	*p*-value
2000	0.481***	0.000	2010	0.393***	0.000
2001	0.470***	0.000	2011	0.387***	0.000
2002	0.454***	0.000	2012	0.390***	0.000
2003	0.435***	0.000	2013	0.343***	0.000
2004	0.434***	0.000	2014	0.302***	0.000
2005	0.456***	0.000	2015	0.321***	0.000
2006	0.464***	0.000	2016	0.347***	0.000
2007	0.461***	0.000	2017	0.353***	0.000
2008	0.424***	0.000	2018	0.356***	0.000
2009	0.420***	0.000	2019	0.363***	0.000

Note: *** denotes the passing of the significance test at a 1 % level.

Table 3
The results of the tests.

	Coefficient	*p*-value
Wald_spatial_lag	799.876***	0.000
LR_spatial_lag	754.399***	0.000
Wald_spatial_error	242.415***	0.000
LR_spatial_ error	208.376***	0.000
Hausman	28.349***	0.000

Note: *** denotes passing the significance test at a 1 % level.

To analyze the spatial agglomeration of CE at the county level, Fig. 6 shows the local agglomeration characteristic of CE in 1997, 2005, 2010, and 2019. In 1997, the high–high (HH) agglomeration areas of CE are mainly distributed in the Pearl River Delta, Yangtze River Delta, Shandong Peninsula, Beijing–Tianjin–Hebei, and Northeast regions, with a few areas are distributed in counties of Guizhou, Sichuan, Yunnan, Shangxi, Hubei, Xinjiang, and Inner Mongolia. Low–high (LH) agglomeration areas mainly followed the distribution of HH agglomeration areas. Low–low (LL) agglomeration areas were distributed in most countries in mainland China, including southeastern, northwestern, and southwestern regions. There were very few high–low (HL) agglomeration areas.

In 2005, the spatial pattern of CE did not change significantly. The range of HH agglomeration of CE in the Shandong Peninsula had expanded based on 1997. As a responsible developing country, China has attached great importance to addressing climate change. In 2008, the Chinese government issued *China's Policies and Actions to Address Climate Change*, proposing policies and actions to mitigate climate change. Areas with serious CE have sought to reduce their CE through continuous optimization of industrial structure, improvement of energy efficiency, development of the circular economy, and other measures. Therefore, in 2010, the range of HH agglomeration of CE in the Shandong Peninsula, Beijing–Tianjin–Hebei region, and Yangtze River Delta decreased significantly, while HH agglomeration areas began to agglomerate in central China.

Compared to 1997, the scope of HH agglomeration areas was greatly reduced in the Beijing–Tianjin–Hebei and the Yangtze River Delta. Instead, HH agglomeration areas began to agglomerate on a large scale in central China, such as in Shanxi, Shaanxi, Inner Mongolia, and Ningxia. The main reason is that these regions are rich in coal resources, and the secondary industries account for a high proportion. The Shanxi–Shaanxi–Inner Mongolia–Ningxia region is one of the six major coal-accumulating areas in China [35]. This region (Shaanxi, Inner Mongolia, Ningxia, and Gansu) boasts significant energy and mineral reserves, with proven reserves of coal, oil, and natural gas constituting 19.7 %, 31.7 %, and 29.8 % of the national energy resources, respectively [36]. In addition, its industrial structure has always been dominated by coal resources. Massive energy consumption has led to rising CE levels and accumulation, and this situation will not change in the short term [19]. From 2000 to 2016, the total CE exhibited an upward trend, surging from 0.94×10^{8} t to 6.62×10^{8} t in this regions with an average annual growth rate of 13.2 % [36]. Moreover, some high-polluting enterprises in the eastern regions have relocated to the central region, aggravating CE in the central regions. Likewise, the LH agglomeration areas varied with the HH agglomeration areas, while the changes in LL and HL agglomeration areas are relatively small. In summary, it can be seen that the areas with high CE at the county level in China have begun to shift from the eastern coastal areas to the central areas.

4.3. The influencing factors of carbon emissions and their spatiotemporal heterogeneity

To investigate the influencing factors of CE at a small spatial scale, considering the spatial correlation of CE, we constructed a spatial econometric model. Following the recommendation of LeSage and Pace [37], the spatial Durbin model (SDM) was selected. First, we should judge whether SDM could be simplified into an SLM model or SEM model. According to the Wald test spatial lag ($p = 0.000$), LR test spatial lag ($p = 0.000$), Wald test spatial error ($p = 0.000$), and the LR test spatial error ($p = 0.000$), SDM model should not be simplified to the SLM and SEM model [37] (see Table 3). Therefore, SDM was best. Next, the value of the Hausman test was 28.349, which also passed the significance test at the 1 % level, indicating that a fixed-effect model is better. The fixed effects can be divided into time fixed effects, spatial fixed effects, and spatio-temporal fixed effects. According to the results of R^2 and Log$L$ values

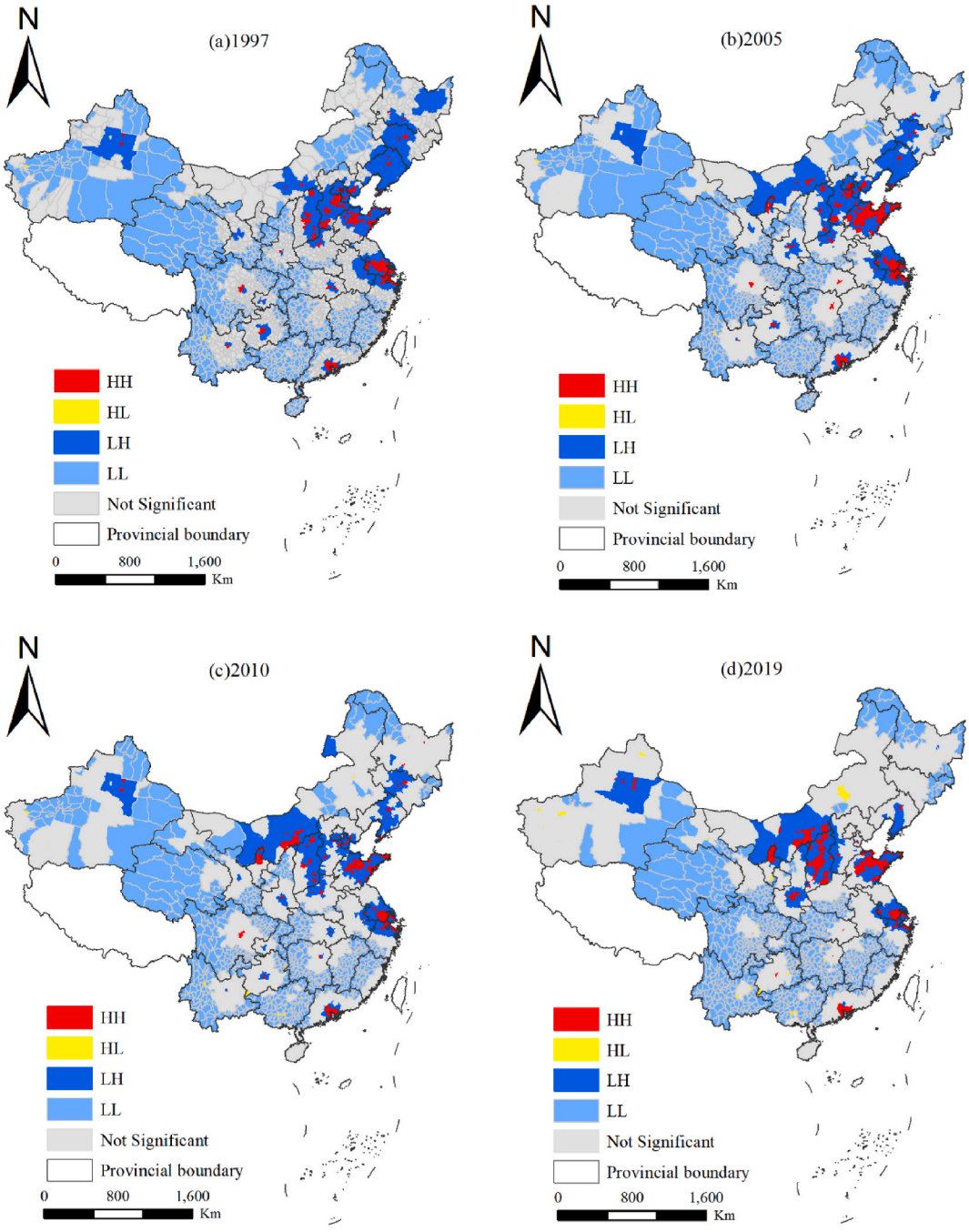

Fig. 6. The local agglomeration patterns of carbon emissions in 1997 and 2019.

undere different effects, the spatio-temporal fixed effect was most optimal.

Table 4 shows the results of the SDM spatio-temporal fixed effects model for mainland China. Due to the limitations of socio-economic statistical data, the regression analysis covered the period from 2000 to 2019. According to the baseline regression results, the spatial lag coefficient was 0.779 ($p = 0.000 < 0.01$). This indicates that CE exhibit spatial spillover effects. Specifically, a 1 % increase in CE in surrounding areas leads to a 0.779 % increase in CE in the local area.

For the influencing factors, the coefficients of PD, CI, and IS were 0.192, 0.151, and 0.056, respectively, and the corresponding *p*-values were all 0.000, indicating that these three influencing factors all have a significant promoting effect on CE. An increase in population density will lead to more industrial and urbanization activities, increasing the demand for energy, especially high-emissions energy, thus affecting CE [38]. In addition, increased population density generally requires more transportation and

Table 4
The results of SDM spatio-temporal fixed effects for mainland China.

	Base	Robustness test	
	Rook adjacency spatial weight matrix	Inverse distances spatial weight matrix	k-NearestNeighbor spatial weight matrix
PD	0.178*** (0.000)	0.202*** (0.000)	0.188*** (0.000)
CI	0.161*** (0.000)	0.229*** (0.000)	0.148*** (0.000)
IS	0.058*** (0.000)	0.082*** (0.000)	0.056*** (0.000)
GS	−0.028*** (0.000)	−0.055*** (0.602)	−0.039*** (0.017)
PGDP	−1.833*** (0.000)	−1.753*** (0.000)	−1.738 (0.000)
PGDP2	0.161*** (0.000)	0.143*** (0.000)	0.151*** (0.000)
PGDP3	−0.005*** (0.000)	−0.004*** (0.000)	−0.004*** (0.000)
W*PD	−0.112*** (0.000)	−0.286*** (0.003)	−0.138*** (0.000)
W*CI	−0.091*** (0.000)	−0.108*** (0.002)	−0.081*** (0.000)
W*IS	−0.029*** (0.000)	−0.070** (0.049)	−0.032*** (0.000)
W*GS	0.001*** (0.000)	0.083*** (0.000)	0.010*** (0.005)
W*PGDP	1.564*** (0.000)	1.156*** (0.000)	1.661*** (0.000)
W*PGDP2	−0.145*** (0.000)	−0.079*** (0.007)	−0.155*** (0.000)
W*PGDP3	0.004*** (0.000)	0.002*** (0.000)	0.005*** (0.000)
ρ	0.779*** (0.000)	0.820*** (0.000)	0.721*** (0.000)
R2	0.979	0.956	0.978
LogL	33566.162	18284.512	32716.53

Note: *** denotes passing the significance test at a 1 % level.

infrastructure, and they also require large amounts of energy [39]. Furthermore, a larger population will generate greater living and production activities, and current energy use mainly relies on coal and other high-energy-consuming energy sources at the county scale in China [14]. Furthermore, increases in population generally do not lead to significant reductions in overall CE through increased energy efficiency or improved lifestyles.

At the city scale, most studies have shown that population density has a significant promoting effect on CE; however, some scholars also pointed out that the impact of population density on CE is not significant in most provinces [27,40–42]. It can be found that there are scale differences in the impact of population density on CE. It is worth noting that, although an increase in PD will increase the local CE, it will have an inhibitory effect on the CE of the surrounding areas. Due to the uneven geographical distribution of population and resources, the agglomeration of local economic and social activities will attract more surrounding populations to the local area, thereby reducing the population density in surrounding areas. The reduction in population density in the surrounding areas will be accompanied by an overall reduction in CE.

CI reflects energy utilization efficiency. The impact of energy utilization efficiency on CE is a complex process involving multiple links [43]. In the energy production process, CE are reduced by using more efficient and cleaner energy production technologies, such as renewable and low-carbon energy. In the process of energy transmission and conversion, efficient energy transmission systems and energy conversion equipment can reduce energy losses during energy transmission and conversion. When energy is ultimately used for heating, power supply, transportation, and so on, improving terminal energy utilization efficiency can reduce energy consumption per unit area, thereby reducing the corresponding CE [39]. Although improvement of energy utilization efficiency can reduce CE, with the development of urbanization and industrialization, the demand for energy increases sharply, and high energy consumption leads to a large volume of CE. The reduction of CE at the county level in China requires continuous adjustment of the energy structure and technological innovation on the basis of improving energy efficiency, in order to effectively reduce CE. Similarly, improvements in local energy efficiency will curb the increase in CE in surrounding areas.

IS has a positive impact on CE. Secondary industries are energy-intensive and has a large demand for high energy-consuming fossil fuels such as coal and oil. The combustion of these energy sources is often accompanied by high CE. Therefore, the development of industrialization has a direct promoting impact on CE [44]. Moreover, industrial production is inevitably accompanied by a series of production activities, including raw material extraction, processing and manufacturing, transportation, and other links, which also produce large amounts of CE. Although industrial development is also accompanied by improvements in technological levels and energy efficiency, in China, due to the rapid advancement of industrialization and the expansion of the production scale, the application of new technologies and improvements in energy efficiency is relatively slow [25], leading to increase in carbon emissions.

Unlike PD, CI, and IS, the coefficient of GS was −0.028 ($p = 0.000 < 0.01$) indicating that GS has a significant inhibitory effect on CE and is beneficial in terms of reducing CE. Part of government fiscal expenditure is often used for ecological environment protection, restoration, and infrastructure construction. Through ecological projects such as afforestation and wetland protection, the carbon sink capacity can be effectively improved and the absorption and fixation of carbon dioxide can be promoted. In addition, government fiscal expenditure can also promote CE reduction actions by enterprises through policy guidance and incentive mechanisms, which is also beneficial for the reduction of CE [45]. However, an increase in local GS can increase CE in surrounding areas.

There exists a non-linear relationship between PGDP and county CE. The results in Table 4 show that the coefficients of PGDP3, PGDP2, and PGDP were negative, positive, and negative, respectively. It shows that PGDP and CE presents an inverted N-shape relationship, which indicates that an increase in PGDP does not necessarily lead to a decrease in CE; that is, the emissions reduction effect of income is unstable. The traditional EKC hypothesis states that there is an inverted U-shaped relationship between CE and economic growth [46]. In recent years, various studies have provided empirical evidence for the existence of N-shaped EKC [47,48]

Table 5
The results of SDM spatio-temporal fixed effects for different regions.

	East	West	Central
PD	0.104*** (0.000)	0.230*** (0.000)	0.255*** (0.000)
CI	0.172*** (0.000)	0.178*** (0.000)	0.113*** (0.000)
IS	0.081*** (0.000)	0.016*** (0.000)	0.071*** (0.000)
GS	−0.046*** (0.000)	−0.001 (0.876)	−0.074*** (0.000)
PGDP	−1.005*** (0.000)	−2.938*** (0.000)	0.110 (0.474)
PGDP2	0.088*** (0.000)	0.269*** (0.000)	−0.053*** (0.000)
PGDP3	−0.003*** (0.000)	−0.008*** (0.000)	0.003*** (0.000)
W*PD	0.050*** (0.004)	−0.252*** (0.000)	−0.119*** (0.000)
W*CI	−0.102*** (0.000)	−0.142*** (0.000)	−0.014* (0.060)
W*IS	−0.032*** (0.000)	−0.030*** (0.000)	−0.021*** (0.001)
W*GS	0.037*** (0.000)	−0.006 (0.446)	−0.031*** (0.003)
W*PGDP	−1.652*** (0.000)	3.402*** (0.000)	0.432 (0.126)
W*PGDP2	0.164*** (0.000)	−0.321*** (0.000)	−0.013 (0.656)
W*PGDP3	−0.005*** (0.000)	0.010*** (0.000)	−0.001 (0.504)
ρ	0.674*** (0.000)	0.725*** (0.000)	0.724*** (0.000)
R2	0.982	0.976	0.976
LogL	12870.839	10997.881	10585.129

Note: *** denotes passing the significance test at a 1 % level.

and inverted N- shaped EKC [21,49,50]. Our results support the existence of an inverted N-shaped EKC for China at the county level. In generally, economic growth affects changes in environmental quality mainly through economic scale, economic structure, and technological progress [21]. At different stages of development, the interactions among these three factors lead to diversity in the relationship between economic growth and CE, ultimately presenting an inverted N-shaped model. After calculation, it is estimated that the turning points of the inverted N-shape EKC were $825.875 and $1,378,455.171 respectively. Most of China's county-level cities are located between the first and second inflection points of PGDP, indicating that CE are expected to continue to rise under the current background of continued growth of PGDP. The relationship between PGDP and CE in surrounding areas shows an opposite trend to that of local CE, showing an N-shaped relationship. To ensure the robustness of the results, we selected the spatial weight matrix of k-NearestNeighbor and the inverse distance for robustness testing. It can be seen that the results did not change significantly under different types of spatial weight matrices, indicating that our research results are robust.

Due to China's vast area and large differences in the level of economic development among regions, its CE are spatially heterogeneous. From the perspective of different regions (Table 5), PD, CI, and IS all had a significant promoting effect on CE in the eastern, central, and western regions, while GS had a significant inhibitory effect on CE for the eastern and western regions, and a non-significant effect on CE in the central region. In addition, the PGDP and CE in the eastern and western regions presented an inverted N-shaped relationship, while the PGDP and CE in the central region show an N-shaped relationship.

In the early stage of regional development, the level of economic and urbanization development is relatively low. At this time, industries are less-developed, the scale of economic output is small, and the scale effect of economic growth on CE is not obvious. When PGDP crosses the first inflection point, the economy is in a period of rapid expansion, and the reduction in the scale of emissions brought about by technological progress, environmental regulations, and emissions reduction devices cannot offset the increase in the scale of emissions brought about by economic growth. When PGDP reaches the second inflection point, the structural, technological, and spillover effects of economic growth gradually become prominent. Extensive economic growth has gradually shifts to intensive economic growth, the technological level of enterprises improves, cleaner production is achieved, and energy consumption is reduced. Therefore, after entering this stage, economic growth will have a significant inhibitory effect on CE. Therefore, the PGDP and CE in the eastern and western regions present an inverted N-shaped relationship.

The central counties are rich in energy and various metal and non-metal mineral resources. Their coal reserves account for 80 % of China's total, and they also has a good heavy industry foundation. This may have led to greater reliance on these high-carbon resources (e.g., coal and metallic and non-metallic minerals) in the early stage of industrialization. The extraction and utilization of these resources may result in high CE during the start-up phase of the economy. This leads to an increase in CE accompanying the initial growth in GDP per capita. When the economy reaches a certain stage of development, counties in the central region may seek industrial upgrading and structural transformation towards cleaner and higher value-added industries, and CE begin to decline. While pursuing higher economic growth, some localities may face increased energy demand to meet the need of the expanding industrial scale, transportation, and urban population, leading to high energy consumption and CE.

5. Discussion

The study of CE at the county level is of great significance for the reduction of CE and the formulation of related policies. For this study, CE at the county level in mainland China were calculated based on DMSP-OLS and NPP-VIIRS nighttime light data. Then, the spatiotemporal changes and influencing factors of CE were explored, which yielded some interesting findings.

Obtaining long-time CE data at small spatial scales has always been a key challenge for scholars to conduct relevant research, limiting the in-depth understanding of CE trends and influencing factors [9]. This study obtained long time-series CE at the county

level in mainland China based on DMSP-OLS and NPP-VIIRS nighttime light data inversion. In contrast to previous studies [16–18], first, a MLP deep learning method was used to inter-calibrate the DMSP-OLS and NPP-VIIRS nighttime light data. Compared with the linear regression or shallow neural network methods used by most scholars, the MLP method can not only effectively identify non-linear relationships between elements but also has higher fitting accuracy.

Second, the correlation coefficient regarding the calibration of DMSP-OLS and NPP-VIIRS nighttime light data was 0.970, which is higher than reported in previous studies [9,14,16,17]. For example, Chen et al. [9] have also obtained the CE data at the county level over mainland China based on DMSP-OLS and NPP-VIIRS nighttime light data, and reported a fitting accuracy of 0.955; Lv et al. [14] have calculated the fitting results of the regression relationship between DMSP-OLS data and NPP-VIIRS composite data at county level in China as 0.835; and Li et al. [16] have simulated DMSP/OLS composites from the VIIRS day-and-night band (DNB) composites by using a power function for radiometric degradation and a Gaussian low-pass filter for spatial degradation, and obtained a fitting accuracy of 0.910. The DMSP/OLS data and the simulated DMSP/OLS data were combined to estimate the city light dynamics in Syria's major human settlements. Moreover, to finally obtain county-level CE, we also simulated the inter-calibrated nighttime light data and actual CE at the provincial level using the MLP method, and obtained a fitting accuracy of 0.996, higher than the values of 0.990, 0.940, and 0.692 reported by Chen et al. [9], Meng et al. [33], and Lv et al. [14]. This further illustrates that our results yielded improved accuracy over previous studies when considering CE at the county level.

Based on the obtained county-level CE, we explored the associated influencing factors. On one hand, our study enriches the discussion of factors affecting CE at small spatial scales. On the other hand, our results indicated that the relationship between PGDP and CE is an inverted N-shaped relationship, challenging the mainstream wisdom that there exists a linear relationship or an inverted U-shaped relationship between PGDP and CE [44,51,52]. Previous studies have also explored the relationship between PGDP and CE [53–55], and varying opinions were put forward. For example, Qi et al. [54] found that there was no decoupling relationship between county per capita GDP and CE in Zhejiang province; Wang et al. [55] have pointed out that PDGP had a positive impact on CE in the Yangtze River Delta; and Zhang et al. [56] also found that PGDP is one of the main factors for the increase in CE in China, even in undeveloped regions. In addition, some scholars have reported an inverted U-shape (or U-shaped) relationship between PGDP and CE in northwest China [57,58]. Most of them have explored the relationship between GDP and CE in specific regions, and the comprehensive understanding of the overall pattern is still limited. To explore the influencing factors, this study used nationwide county-level data, which provides a new perspective for a more comprehensive understanding of China's CE pattern. By introducing the higher-order terms of PGDP ($PGDP^2$ and $PGDP^3$), we observed that there is a non-linear relationship between PGDP and CE, and thus proposed an inverted N-shape conclusion, which provides a new perspective for a deeper understanding of the impact of PGDP on CE. In particular, there are large differences in economic between regions, leading the relationship between PGDP and CE to be spatially heterogeneous. We found that in some developed regions, PGDP and CE were not decoupled or had a purely linear relationship, which is different from the conclusions of some previous studies [59], and providedimportant clues for a better understanding the regional differences in CE. In addition, we focused on the N-shaped relationship between PGDP and CE in central China, which is not common in the existing literature. This finding suggests that the relationship between PGDP and CE may be more complex and variable than previously thought. Our results highlight the impact of spatial scale on this relationship, suggesting the importance of local characteristics and regional differences in CE patterns.

However, there were still some limitations to the study. On the one hand, the nighttime light data of nine periods from January to May and September to December in the study area were selected for annual synthesis. Mainly as data distortion occurs in the NPP-VIIRS nighttime light data in the middle and high latitudes, and mostly appears in the summer, we selected the annual nighttime light data synthesized from the nine periods of nighttime light data from January to May and September to December in the study area as the basic research data. The period from June to August covers summer, which may contain some data related to factors affecting summer-specific CE, such as air conditioning electricity consumption, summer industrial production, and so on. Ignoring summer data may provide an incomplete explanation of seasonal changes in CE. However, our research was focused on long-term CE trends, and selecting these periods helped to reduce the impact of short-term fluctuations, reduce noise in the nighttime light data, and improve the stability and reliability of the data. As we did not discuss the seasonal changes in CE, it can be considered acceptable to process the data in this way. Additionally, some previous studies [20,60,61] have demonstrated the effectiveness of this approach over similar time periods. However, this data processing method may have imposed certain limitations on the research results by ignoring the data from June to August. Furthermore, this study mainly focused on the spatiotemporal dynamics and influencing factors of CE, but did not conduct an in-depth analysis of specific sources of CE, such as energy, industry, transportation, and so on. A more detailed analysis of the sources of CE may help to formulate more specific emissions reduction policies. In addition, although some factors affecting CE were mentioned in the study, in-depth analysis of the mechanisms and relationships behind these factors remained limited; especially the differences in CE influencing mechanisms at the county level, the prefecture level, city level, and even at a larger spatial scales, which need further exploration.

Based on our results, some policy implementations to reduce CE can be suggested. First, the government should develop regionally differentiated CE reduction policies: given the differences in factors affecting CE in different regions, it is recommended that the government adopt differentiated CE reduction policies, rather than one-size-fits-all policies. Second, urban planning and construction should be strengthened. Based on the positive impact of population density (PD) on CE observed in this study, it is recommended that the government focus on improving energy efficiency and promoting low-carbon transportation methods in urban planning and construction, as well as encouraging the development of green buildings and urban public transportation systems to reduce reliance on high-carbon transportation and energy-intensive buildings. Third, in terms of energy structure adjustment and technological innovation, given the significant impact of IS and CI on CE, the government should promote industrial upgrading and encourage the application of cleaner production technologies. This will support the development of new and renewable energy, reduce dependence

on high-carbon energy, and promote more sustainable development. Finally, regarding the effective use of public financial investment, as GS presented an inhibitory effect on CE, it is recommended that the government increase investment into environmental protection, infrastructure, and public services. In particular, investment in environmental sanitation, transportation infrastructure, and ecological and environmental protection projects can generate positive external economic benefits and promote the reduction of CE.

6. Conclusion

Based on nighttime light remote sensing data, this study retrieved the long-term CE inventory at the county level in mainland China by fusing two types of nighttime light data. On this basis, this study analyzes the spatiotemporal evolution characteristics and influencing factors of CE at the county level in mainland China, and further explores the temporal and spatial differences of influencing factors. The main conclusions are as follows:

1. We obtained long-term (1997–2019) CE data at the county level in mainland China through inversion of nighttime light data, and the period of the time series is longer than previous studies, and the inversion accuracy was $r^2 = 0.996$, which was higher than previous research results.
2. There is a positive spatial correlation in county-level CE. In terms of time, the spatial correlation is gradually weakening as time goes by. In terms of space, the center of CE gradually shifts from the eastern coastal area to the central regions.
3. Overall, PD, IS, and CI all had a significant promoting effect on CE, GS had a significant inhibitory effect, and PGDP had an inverted-N relationship with CE. However, there are differences in the influencing factors of county-level CE in different regions and periods. Among them, GS has a significant inhibitory effect in the eastern and central regions, while the effect on CE in the western region is insignificant. PGDP shows an inverted N-shaped relationship with CE in the eastern and western regions and an N-shaped relationship in the central region.

Data availability statement

Data will be made available on request.

Funding

This work was funded by the Shanghai Social Science Foundation of China (grant number 2022ECK005).

CRediT authorship contribution statement

Nina Zhu: Writing – review & editing, Writing – original draft, Visualization, Validation, Software, Resources, Methodology, Investigation, Funding acquisition, Formal analysis, Data curation, Conceptualization. **Xue Li:** Formal analysis, Conceptualization. **Sibo Yang:** Supervision, Project administration, Investigation, Formal analysis, Conceptualization. **Yi Ding:** Resources, Investigation, Data curation. **Gang Zeng:** Formal analysis, Data curation.

Declaration of competing interest

The authors declare that they have no known competing financial interests or personal relationships that could have appeared to influence the work reported in this paper.

References

[1] D.A. Lashof, D.R. Ahuja, Relative contributions of greenhouse gas emissions to global warming, Nature 344 (6266) (1990) 529–531, https://doi.org/10.1038/344529a0.
[2] F. Mao, Z. Li, K. Zhang, Carbon dioxide emissions estimation of conventional diesel buses electrification: a well-to-well analysis in Shenzhen, China, J. Clean. Prod. 277 (2020) 123048, https://doi.org/10.1016/j.jclepro.2020.123048.
[3] S. Shao, Y. Chen, K. Li, L. Yang, Market segmentation and urban CO2 emissions in China: evidence from the Yangtze River Delta region, J. Environ. Manag. 248 (2019) 109324, https://doi.org/10.1016/j.jenvman.2019.109324.
[4] C. Bai, C. Feng, H. Yan, X. Yi, Z. Chen, W. Wei, Will income inequality influence the abatement effect of renewable energy technological innovation on carbon dioxide emissions? J. Environ. Manag. 264 (2019) 110482 https://doi.org/10.1016/j.jenvman.2020.110482.
[5] M.K. Khan, M.I. Khan, M. Rehan, The relationship between energy consumption, economic growth and carbon dioxide emissions in Pakistan, Financial, Innovation 6 (1) (2020) 1–13, https://doi.org/10.1186/s40854-019-0162-0.
[6] D. Toebelmann, T. Wendler, The impact of environmental innovation on carbon dioxide emissions, J. Clean. Prod. 244 (2020) 118787, https://doi.org/10.1016/j.jclepro.2019.118787.
[7] Z. Xu, L. Liu, L. Wu, Forecasting the carbon dioxide emissions in 53 countries and regions using a non-equigap grey model, Environ. Sci. Pollut. R. 28 (13) (2021) 15659–15672, https://doi.org/10.1007/s11356-020-11638-7.
[8] J. Li, X. Huang, X. Chuai, H. Yang, The impact of land urbanization on carbon dioxide emissions in the Yangtze River Delta, China: a multiscale perspective, Cities 116 (2021) 103275, https://doi.org/10.1016/j.cities.2021.103275.
[9] J. Chen, M. Gao, S. Cheng, W. Hou, M. Song, X. Liu, Y. Liu, Y. Shan, County-level CO2 emissions and sequestration in China during 1997–2017, Sci. Data 7 (2020) 391, https://doi.org/10.1038/s41597-020-00736-3.
[10] Z. Long, Z. Zhang, S. Liang, X. Chen, B. Ding, B. Wang, Y. Chen, Y. Sun, S. Li, T. Tang, Spatially explicit carbon emissions at the county scale, Resour. Conserv. Recycl. 173 (2021) 105706, https://doi.org/10.1016/j.resconrec.2021.105706.

[11] W. Cao, X. Yuan, Region-county characteristic of spatial-temporal evolution and influencing factor on land use-related CO2 emissions in Chongqing of China, 1997–2015, J. Clean. Prod. 31 (2019) 619–632, https://doi.org/10.1016/j.jclepro.2019.05.248.
[12] Y. Guan, L. Kang, C. Shao, P. Wang, M. Ju, Measuring county-level heterogeneity of CO2 emissions attributed to energy consumption: a case study in Ningxia Hui Autonomous Region, China, J. Clean. Prod. 142 (2017) 3471–3481, https://doi.org/10.1016/j.jclepro.2016.10.120.
[13] D. Yang, W. Luan, L. Qiao, M. Pratama, Modeling and spatio-temporal analysis of city-level carbon emissions based on nighttime light satellite imagery, Appl. Energ. 268 (2020) 114696, https://doi.org/10.1016/j.apenergy.2020.114696.
[14] Q. Lv, H. Liu, J. Wang, H. Liu, Y. Shang, Multiscale analysis on spatiotemporal dynamics of energy consumption CO2 emissions in China: utilizing the integrated of DMSP-OLS and NPP-VIIRS nighttime light datasets, Sci. Total Environ. 703 (2020) 134394, https://doi.org/10.1016/j.scitotenv.2019.134394.
[15] C. Zuo, W. Gong, Z. Gao, D. Kong, R. Wei, X. Ma, Correlation analysis of CO2 concentration based on DMSP-OLS and NPP-VIIRS integrated data, Remote. Sens-Basel. 14 (17) (2022) 4181, https://doi.org/10.3390/rs14174181.
[16] X. Li, D. Li, H. Xu, C. Wu, Intercalibration between DMSP/OLS and VIIRS night-time light images to evaluate city light dynamics of Syria's major human settlement during Syrian Civil War, Int. J. Remote. Sens. 38 (2017) 5934–5951, https://doi.org/10.1080/01431161.2017.1331476.
[17] J. Zhao, G. Ji, Y.L. Yue, Z. Lai, Y. Che, D. Yang, X. Yang, Z. Wang, Spatio-temporal dynamics of urban residential CO2 emissions and their driving forces in China using the integrated two nighttime light datasets, Appl. Energ. 235 (2019) 612–624, https://doi.org/10.1016/j.apenergy.2018.09.180.
[18] J.J. Ma, J.Y. Guo, S. Ahmad, Z. Li, J. Hong, Constructing a new inter-calibration method for dmsp-ols and npp-viirs nighttime light, Remote. Sens-basel. 12 (6) (2020) 937, https://doi.org/10.3390/rs12060937.
[19] X.N. Li, Y. Feng, P.Y. Wu, Y. Chiu, An analysis of environmental efficiency and environmental pollution treatment efficiency in China's industrial sector, Sustainability-basel 13 (5) (2021) 2579, https://doi.org/10.3390/su13052579.
[20] X.Y. Wang, Research on the Change of Urban Spatial Pattern in Shandong Province Based on NPP/VIIRS, Xi'an university of science and technology, 2021.
[21] P. Zhang, Y. Jia, J. Gao, W. Song, H. Leung, Short-term rainfall forecasting using multi-layer perceptron, IEEE T Big Data 6 (2018) 93–106, https://doi.org/10.1109/TBDATA.2018.2871151.
[22] J.T. Esteves, G. de Souza Rolim, A.S. Ferraudo, Rainfall prediction methodology with binary multilayer perceptron neural networks, Clim. Dynam. 52 (2019) 2319–2331, https://doi.org/10.1007/s00382-018-4252-x.
[23] Q. Ran, J. Zhang, Y. Hao, Does environmental decentralization exacerbate China's carbon emissions? Evidence based on dynamic threshold effect analysis, Sci. Total Environ. 721 (2020) 137656, https://doi.org/10.1016/j.scitotenv.2020.137656.
[24] F. Xu, Q. Huang, H. Yue, C. He, C. Wang, H. Zhang, Reexamining the relationship between urbanization and pollutant emissions in China based on the STIRPAT model, J. Environ. Manag. 273 (2020) 111134, https://doi.org/10.1016/j.jenvman.2020.111134.
[25] J. Huang, X. Li, Y. Wang, H. Lei, The effect of energy patents on China's carbon emissions: evidence from the STIRPAT model, Technol. Forecast. Soc. 173 (2021) 121110, https://doi.org/10.1016/j.techfore.2021.121110.
[26] Z. Cao, Z. Wu, S. Mi, K. Yang, A method for classified correction of stable DMSP/OLS nighttime light imagery across China, Journal. Of. Geo-information. Science. 22 (2020) 246–257 (in Chinese).
[27] C. Zhang, Z. Tan, The relationships between population factors and China's carbon emissions: does population aging matter? Renew. Sust. Energ. Rev. 65 (2016) 1018–1025, https://doi.org/10.1016/j.rser.2016.06.083.
[28] X. Cao, Y. Hu, X. Zhu, F. Shi, L. Zhuo, J. Chen, A simple self-adjusting model for correcting the blooming effects in DMSP-OLS nighttime light images, Remote Sens. Environ. 24 (2019) 401–411, https://doi.org/10.1016/j.rse.2019.02.019.
[29] Q. Liu, J. Fan, J. Zuo, P. Li, Y. Shen, Z. Ren, Y. Zhang, A spatiotemporally constrained interpolation method for missing pixel values in the suomi-NPP VIIRS monthly composite images: taking Shanghai as an example, Remote. Sensing-basel. 15 (9) (2023) 2480, https://doi.org/10.3390/rs15092480.
[30] Y. Wu, K. Shi, B. Yu, C. Li, Analysis of the impact of urban sprawl in haze pollution based on the NPP-VIIRS nighttime light remote sensing data, Geomatric and information science of Wuhan university 46 (2021) 777–789, https://doi.org/10.13203/j.whugis20200455, 05.
[31] Y. Wang, C. Huang, M. Zhao, J. Hou, Y. Zhang, J. Gu, Mapping the population density in mainland China using NPP/VIIRS and points-of-interest data based on a random forests model, Remote Sens-basel 12 (2020) 3645, https://doi.org/10.3390/rs12213645.
[32] A. Shortland, K. Christopoulou, C. Makatsoris, War and famine, peace and light? The economic dynamics of conflict in Somalia 1993–2009, J. Peace Res. 50 (2013) 545–561, https://doi.org/10.1177/0022343313492991.
[33] L. Meng, W. Graus, E. Worrell, B. Huang, Estimating CO2 (carbon dioxide) emissions at urban scales by DMSP/OLS (Defense Meteorological Satellite Program's Operational Linescan System) nighttime light imagery: methodological challenges and a case study for China, Energy 71 (2014) 468–478, https://doi.org/10.1016/j.energy.2014.04.103.
[34] Y. Su, X. Chen, Y. Li, Y. Ye, H. Zhang, N. Huang, Y. Kuang, China's 19-year city-level carbon emissions of energy consumptions, driving forces and regionalized mitigation guidelines, Renew. Sust. Energ. Rev. 35 (2014) 231–243, https://doi.org/10.1016/j.rser.2014.04.015.
[35] Y. Wang, X. Bai, L. Wu, Y. Zhang, S. Qu, The petrographic compositions of Chinese commercial coals: a national survey and statistical analysis, Fuel 310 (2020) 122323, https://doi.org/10.1016/j.fuel.2021.122323.
[36] X. Han, J. Yu, Y. Xia, J. Wang, Spatiotemporal characteristics of carbon emissions in energy-enriched areas and the evolution of regional types, Energy Rep. 7 (2021) 7224–7237, https://doi.org/10.1016/j.egyr.2021.10.097.
[37] J. LeSage, R.K. Pace, Introduction to Spatial Econometrics, Chapman and Hall/CRC, New York, 2009, https://doi.org/10.1177/0160017612452429.
[38] L. Han, W. Zhou, W. Li, Y. Qian, Urbanization strategy and environmental changes: an insight with relationship between population change and fine particulate pollution, Sci. Total Environ. 642 (2018) 789–799.
[39] X. Meng, J. Han, Roads, economy, population density, and CO2: a city-scaled causality analysis, Resour. Conserv. Recycl. 128 (2018) 508–515, https://doi.org/10.1016/j.resconrec.2016.09.032.
[40] Y. Wu, V.W.Y. Tam, C. Shuai, L. Shen, Y. Zhang, S. Liao, Decoupling China's economic growth from carbon emissions: empirical studies from 30 Chinese provinces (2001–2015), Sci. Total Environ. 656 (2019) 576–588, https://doi.org/10.1016/j.scitotenv.2018.11.384.
[41] I.M. Zarco-Soto, P.J. Zarco-Periñán, R. Sánchez-Durán, Influence of cities population size on their energy consumption and CO2 emissions: the case of Spain, Environ. Sci. Pollut. R. 28 (2021) 28146–28167, https://doi.org/10.1007/s11356-021-12624-3.
[42] J. Liu, M. Li, Y. Ding, Econometric analysis of the impact of the urban population size on carbon dioxide (CO2) emissions in China, Environ. Dev. Sustain. 3 (12) (2021) 18186–18203, https://doi.org/10.1007/s10668-021-01433-w.
[43] H. Mikulčić, I.R. Skov, D.F. Dominković, S.R.W. Alwi, Z.A. Manan, R. Tan, N. Duić, S.N.H. Mohamad, W. Wan, Flexible Carbon Capture and Utilization technologies in future energy systems and the utilization pathways of captured CO2, Renew. Sust. Energ. Rev. 114 (2019) 109338, https://doi.org/10.1016/j.rser.2019.109338.
[44] B. Aslam, J. Hu, S. Shahab, A. Ahmad, M. Saleem, S. Shoai, A. Shah, M.S. Javed, M.K. Aslam, S. Hussain, M. Hassan, The nexus of industrialization, GDP per capita and CO2 emission in China, Environ. Technol. Innov. 23 (2021) 101674, https://doi.org/10.1016/j.eti.2021.101674.
[45] X. Liu, J. Cifuentes-Faura, S. Zhao, L. Wang, Government environmental attention and carbon emissions governance: firm-level evidence from China, Econ. Anal. Policy 80 (2023) 121–142, https://doi.org/10.1016/j.eap.2023.07.016.
[46] G.M. Grossman, A.B. Krueger, Environmental impacts of a North American free trade agreement. https://doi.org/10.3386/w3914, 1991.
[47] S.A. Churchill, J. Inekwe, K. Ivanovski, R. Smyth, The environmental kuznets curve in the OECD: 1870–2014, Energy Econ. 75 (2018) 389–399, https://doi.org/10.1016/j.eneco.2018.09.004.
[48] S. Rej, B. Nag, Investigating the role of capital formation to achieve carbon neutrality in India, Environ. Sci. Pollut. R. 29 (2022) 60472–60490, https://doi.org/10.1007/s11356-022-20109-0.
[49] A.N. Ajmi, S. Hammoudeh, D.K. Nguyen, J.R. Sato, On the relationships between CO2 emissions, energy consumption and income: the importance of time variation, Energy Econ. 49 (2015) 629–638, https://doi.org/10.1016/j.eneco.2015.02.007.
[50] Y.Q. Kang, T. Zhao, Y.Y. Yang, Environmental Kuznets curve for CO2 emissions in China: a spatial panel data approach, Ecol. Indicat. 63 (2016) 231–239, https://doi.org/10.1016/j.ecolind.2015.12.011.

[51] J.I. Mikayilov, F.J. Hasanov, M. Galeotti, Decoupling of CO2 emissions and GDP: a time-varying cointegration approach, Ecol. Indicat. 95 (2018) 615–628, https://doi.org/10.1016/j.ecolind.2018.07.051.
[52] M. Hatmanu, C. Cautisanu, A.O. Iacobuta, On the relationships between CO2 emissions and their determinants in Romania and Bulgaria. An ARDL approach, Appl. Econ. 54 (22) (2022) 2582–2595, https://doi.org/10.1080/00036846.2021.1998328.
[53] Z. Long, J. Pang, S. Li, J. Zhao, T. Yang, X. Chen, Z. Zhang, Y. Sun, L. Lang, N. Wang, H. Shi, B. Wang, Spatiotemporal variations and structural characteristics of carbon emissions at the county scale: a case study of Wu'an City, Environ. Sci. Pollut. R. 29 (43) (2022) 65466–65488, https://doi.org/10.1007/s11356-022-20433-5.
[54] H. Qi, X. Shen, F. Long, M. Liu, X. Gao, Spatial–temporal characteristics and influencing factors of county-level carbon emissions in Zhejiang Province, China, Environ. Sci. Pollut. R. 30 (4) (2023) 10136–10148, https://doi.org/10.1007/s11356-022-22790-7.
[55] S. Wang, Y. Li, F. Li, D. Zheng, J. Yang, E. Yu, Spatialization and driving factors of carbon budget at county level in the Yangtze River Delta of China, Environ. Sci. Pollut. R. (2023) 1–20, https://doi.org/10.1007/s11356-023-28917-8.
[56] W. Zhang, P. Shi, W. Huang, Research on spatial and temporal pattern evolution and driving factors of county carbon emissions in underdeveloped regions: Gansu province of western China as an example, Sustainability-basel 15 (1) (2022) 291, https://doi.org/10.3390/su15010291.
[57] Z. Zoundi, CO2 emissions, renewable energy and the Environmental Kuznets Curve, a panel cointegration approach, Renew. Sust. Energ. Rev. 72 (2017) 1067–1075, https://doi.org/10.1016/j.rser.2016.10.018.
[58] E. Dogan, R. Inglesi-Lotz, The impact of economic structure to the environmental Kuznets curve (EKC) hypothesis: evidence from European countries, Environ. Sci. Pollut. R. 27 (2020) 12717–12724, https://doi.org/10.1007/s11356-020-07878-2.
[59] L. Mai, Q. Ran, H. Wu, A LMDI decomposition analysis of carbon dioxide emissions from the electric power sector in Northwest China, Nat. Resour. Model. 33 (4) (2020) e12284, https://doi.org/10.1111/nrm.12284.
[60] R. Wu, J. Wang, S. Wang, K. Feng, The drivers of declining CO2 emissions trends in developed nations using an extended STIRPAT model: a historical and prospective analysis, Renew. Sus. Energ. Rev. 149 (2021) 111328, https://doi.org/10.1016/j.rser.2021.111328.
[61] S. Xia, H. Shao, H. Wang, W. Xian, Q. Shao, Z. Yin, J. Qi, Spatio-temporal dynamics and driving forces of multi-scale CO2 emissions by integrating DMSP-OLS and NPP-VIIRS data: a case study in Beijing-Tianjin-Hebei, China, Remote, Sens-basel. 14 (19) (2022) 4799, https://doi.org/10.3390/rs14194799.